

On the Origin of Solar Wind MHD Turbulence: Helios Data Revisited

ROLAND GRAPPIN AND ANDRE MANGENEY

Observatoire de Paris-Meudon, Meudon, France

ECKART MARSCH

Max-Planck-Institut für Aeronomie, Katlenburg-Lindau, Federal Republic of Germany

We study the fluctuations of density, magnetic and velocity fields in the frequency range from $(1 \text{ day})^{-1} = 1.2 \times 10^{-5} \text{ Hz}$ to $(2.8 \text{ min})^{-1} = 6 \times 10^{-3} \text{ Hz}$, as measured by the primary Helios mission (118 days), at heliocentric distances ranging from 0.3 to 1 AU. We address the question of the existence of nonlinear cascades in the observed turbulence, possibly separate for the two "inward" and "outward" components, corresponding to opposite directions of propagation along the large-scale magnetic field. We consider energies per unit mass, not per unit volume, in order to work with variables which are not very sensitive to the heliocentric distance variations. We find that while the whole spectrum of total (kinetic plus magnetic) turbulent energy undergoes very large daily variations both in its amplitude and spectral shape the instantaneous spectrum follows a power law in the frequency range 10^{-4} to $6 \times 10^{-3} \text{ Hz}$. We show that both the amplitude and the spectral index m depend on the proton temperature, in a monotonic way, so that a large temperature (thermal speed about 60 km/s) leads to a low level of turbulence with a steep, Kolmogorov-like spectrum ($m \approx -1.8$), while a low temperature (thermal speed about 16 km/s) leads to a flatter spectrum ($m \approx -1.2$) with a high level of turbulence. This relation is independent from heliocentric distance, at least between 0.3 and 1 AU. Decomposing the turbulent energy into two components, "outward" and "inward," we find that the spectrum of the outward component also follows very closely the daily proton temperature variations, while the inward component's spectrum is less sensitive to the temperature but also varies with the relative level of rms proton density fluctuations. As a consequence, Alfvénic periods (in which energy is dominated by the outgoing component) occur mainly when density fluctuations are low and temperature is high, which does not contradict the classical view that they are found in the "trailing edges of high-speed streams" (Belcher and Davis, 1971). The existence of inertial ranges controlled by the level of density fluctuations is not completely new (see the numerical simulations of purely hydrodynamic turbulence by Pouquet and Passot (1987)), but the strong dependence of both turbulent energy level and spectral slope on temperature is a new, unexpected property of solar wind turbulence which remains to be explained.

1. INTRODUCTION

The inner solar wind is a strongly inhomogeneous plasma expanding at supersonic velocity and as such does not appear to be a very good candidate for testing theoretical ideas concerning MHD turbulence. However, the spectra of velocity and magnetic field fluctuations strongly suggest fully developed turbulence covering several decades of frequencies. Coleman [1968] was the first to follow this idea and to suggest that these spectra resulted from an MHD cascade, the most convincing argument being that the slope of the observed spectrum of the magnetic fluctuations was consistent with the $-3/2$ value predicted by Kraichnan [1965] a few years before.

In Kraichnan's theory the turbulent fields are assumed to be a mixture of Alfvén waves propagating in opposite directions along the average magnetic field. Among the various inviscid invariants of incompressible MHD which can determine the properties of the nonlinear cascade, Kraichnan considered one, the total, kinetic plus magnetic energy e . There is, however, another invariant which may

play a considerable role in the nonlinear cascade, namely the velocity-magnetic field correlation e^c . Another very convenient way to express the existence of these two invariants is to use the Elsässer variables $z^\pm = \delta v \pm \delta b$, where δv is the velocity fluctuation and δb is the magnetic field fluctuation normalized to $(4\pi\rho)^{1/2}$, ρ being the mass density. The two energies $e^\pm = \langle |z^\pm|^2 \rangle / 2$ form a couple of inviscid invariants equivalent to e and e^c (Dobrowolny *et al.*, 1980b), which present the advantage of being both definite positive quantities. Thus we may expect both e^\pm spectra to exhibit spectral shapes of their own [see Grappin *et al.* 1983; Pouquet *et al.* 1988]; the case studied by Kraichnan [1965] is then recovered only when $e^+ = e^-$, i.e., when there is no correlation between δv and δb , $e^c = 0$.

In the solar wind, this correlation is often very high, i.e., one observes quite often either $e^+ \gg e^-$, or $e^- \gg e^+$, depending on the direction of the average magnetic field. This has been interpreted by Belcher and Davis [1971] as evidence for the dominance of Alfvén waves propagating along the average spiral magnetic field away from the Sun. Indeed, in the linear case (small amplitude of the fluctuations) e^+ and e^- are the energies in waves traveling in opposite directions along the average magnetic field. In the nonlinear case, it should be stressed that this remains strictly valid only when one of the wave modes is present; in this case, the nonlinear terms vanish, at least in the incompressible limit. Thus as

Copyright 1990 by the American Geophysical Union.

Paper number 89JA03350
0148-0227/90/89JA-03350\$05.00

remarked by *Dobrowolny et al.* [1980a, b], Kraichnan's theory cannot explain the observed well-developed spectrum of outgoing waves since both outgoing and ingoing waves are necessary to have nonlinear interactions and to produce a continuous spectrum. This led these authors to propose that in incompressible decaying MHD turbulence, the nonlinear cascade would amplify any initial unbalance (presumably in favor of outgoing waves in the solar wind), leading asymptotically to a frozen turbulence with just one type of modes present, i.e., with either $\delta v = \delta b$ or $\delta v = -\delta b$. This process of dynamic alignment has since been fully confirmed by numerical experiments [*Grappin et al.*, 1982; *Matthaeus et al.*, 1983; *Pouquet et al.*, 1986; *Grappin*, 1986].

However, there are several counterarguments against the nonlinear origin of the dominance of the outward mode in the solar wind. First, the bulk velocity of the wind is large enough so that the energy-containing eddies have little time to interact nonlinearly, if at all, during the travel time from the Sun's surface to the orbit of the Earth. Thus the initial spectrum of the waves cannot have been substantially modified by nonlinear interactions during that time, at least at the largest scales (see *Grappin et al.* [1982]). Second, even if sufficient time is allowed for the nonlinear interactions to proceed, as is the case at greater distances from the Sun, the nonlinear effects will not necessarily result in an increase of the correlation between δv and δb . Indeed, for the dynamic alignment effect to occur, the large energy-containing scales must have a definite nonzero correlation, while in the solar wind these large scales essentially contain velocity differences between fast and slow streams, i.e., purely kinetic energy for which by definition $e^+ = e^-$. Any preestablished imbalance at medium scales will be swept out by the nonlinear cascade of energy flowing from the isotropic large scales (see the simulations by *Roberts and Goldstein* [1988]).

These arguments are in favor of a simple explanation in which the spectra observed up to the Earth's orbit are formed close to the solar surface, and the dominance of the outward mode is due to the loss of all ingoing waves in the acceleration region of the solar wind [*Belcher and Davis*, 1971].

Does that mean that there are no nonlinear effects to be observed in the solar wind within 1 AU? The answer should be no, since at a given distance from the Sun, there are small enough scales below which nonlinear interactions, whose time scale decreases with the scale length, have had time enough to play a role in the formation of the observed spectrum. The variation of this critical scale could explain the evolution of the energy spectrum with heliocentric distance, as observed by *Denskat and Neubauer* [1982] and *Bavassano et al.* [1982]. Since the medium is inhomogeneous, one expects a competition between nonlinear effects and refractive effects in the vicinity of the critical scale. This competition has been studied by *Tu et al.* [1984] and *Tu* [1988] who succeeded in reproducing some of the observed variations of the spectrum with distance, namely, assuming a flat spectrum at short distances ($\propto k^{-1}$), to produce a Kolmogorov-like (steeper) spectrum at larger distances.

In this paper, of which a short preliminary account was given by *Grappin et al.* [1989], we address the question of whether or not there is any conclusive evidence in the

observations taken within 1 AU of a nonlinear cascade in a restricted range of small scales. Some of the other questions we would like to answer are: is the so-called Alfvénic turbulence really of a different nature than that occurring in non-Alfvénic periods? What are the real differences near the Sun and near the Earth? We shall use the data obtained during the first 4 months of the Helios mission, which covered the range of heliocentric distances between 0.3 and 1 AU, and for which we have at our disposal the merged magnetic and plasma data. The solar activity cycle was at one of its minima, and the source conditions were relatively steady, with mainly two recurrent corotating high-speed streams [see *Burlaga et al.*, 1978].

We shall analyze these data in terms of the Elsässer variables introduced above, because they occur naturally in the theory of incompressible turbulence. This is not the usual way to analyze the data, but we hope to convince the reader that it is fruitful.

The plan of the paper is as follows. Section 2 deals with data analysis and notations, section 3 with global properties of the solar wind and its turbulence during the period considered, section 4 with day-to-day spectral variations (of shape and amplitude). Section 5 presents a discussion, and section 6 a conclusion.

2. DATA ANALYSIS AND NOTATIONS

The data set consists of merged magnetic field data [*Musmann et al.*, 1977] and plasma data [*Rosenbauer et al.*, 1977] obtained during the first 118 days of the primary Helios mission. At a given time, the basic data consist of the proton density, the three components of the plasma bulk velocity and of the magnetic field. The sampling time is of the order of 40 s. We first perform a smoothing by interpolating the existing data linearly at a sampling rate of 1.4 min. Data gaps, which are infrequent during this first part of the Helios mission, were replaced by zeros. We thus obtain for each day a time series of 1024 points, from which we build two kinds of time series with 118 points (one for each day). On the one hand, we compute daily averages and rms quantities; on the other hand, we take the Fourier transform of the original time series on the fundamental period of 1 day. The corresponding 512 frequencies were grouped into nine logarithmically spaced frequency bands from $f_1 = (\text{day})^{-1} \approx 1.2 \times 10^{-5}$ Hz to the Nyquist frequency $f_{\text{max}} = 2^9 f_1 \approx (3 \text{ min})^{-1} \approx 6 \times 10^{-3}$ Hz. The first band Δf_1 contains only the fundamental frequency f_1 , while the others are the eight octaves (with $i=2$ to 9):

$$\Delta f_i = [2^{i-1} f_1, 2^i f_1] \quad (1)$$

The nine characteristic frequencies associated with these bands are f_i and for $i=2$ to 9:

$$f_i = 2^i f_1 / \sqrt{2} \quad (2)$$

We thus obtain for each field (velocity, magnetic field and density) nine time series of 118 points, each corresponding to the energy density in one of the nine bands. We will denote by e_i the energy density at frequency f_i , averaged over the frequency band Δf_i .

The choice of the day as our fundamental period, between the smallest time scale (2.8 min) and the largest (118 days) is a compromise. On the one hand, 1 day is large enough to

allow for 9 octaves of frequency range down to the smallest time scale available, i.e., a little less than 3 orders of magnitude. On the other hand, one day is short enough to let us follow the variation of turbulent properties inside the main characteristic structure of the solar wind, namely the stream structure, which typically lasts about 6 days [see *Burlaga et al.*, 1978].

Let us give now some notations. We denote respectively by δn , δv and δb the fluctuating proton density, velocity and normalized magnetic field fluctuations: $\delta b = \delta B / (4\pi\rho)^{1/2}$, δB and ρ being the magnetic field fluctuation and the proton mass density, respectively. In the following, ρ° and B° are the daily averages of the proton mass density and magnetic field vector, respectively, and B° is $|B^\circ|$. Two exact solutions of the full incompressible ($\delta n = 0$) MHD equations in a uniform field B° are either $z^+ = v + b = 0$, or $z^- = v - b = 0$. They are the so-called linear Alfvén waves (they are linear since the nonlinear terms of the incompressible MHD equations vanish when either z^- or z^+ vanish). The first solution (pure z^-) propagates along the uniform magnetic field B° , and the second solution (pure z^+) propagates backwards. We denote by $e^V = \langle \delta v^2 \rangle / 2$ and $e^M = \langle \delta b^2 \rangle / 2$ the kinetic and magnetic energies per unit mass and energies in both Alfvén modes by $e^\pm = \langle (\delta v \pm \delta b)^2 \rangle / 2$. We will also need a notation for the "energy" in relative density fluctuations, which we denote by $e^n = \langle (\delta n)^2 \rangle / \langle n \rangle^2$.

It has long been recognized that the observed correlation between δv and δb can be interpreted as evidence for Alfvénic fluctuations propagating outward. As discussed in the introduction, this is strictly true only in the incompressible limit, and with only one type of modes present. Nevertheless, the observations show at least that the direction of the large-scale magnetic field plays a crucial role in organizing the data. We shall therefore use the conventional terminology, and speak of ingoing (or inward) and outgoing (or outward) components for the fields z^+ or z^- , depending on the sign of the radial component of the large-scale field, B_R° : $z^{\text{out}} = z^{+s}$, $z^{\text{in}} = z^{-s}$, $s = -\text{sign}(B_R^\circ)$. The same conventions will be used for the energies, e^{in} and e^{out} ; note, however, that we have first performed the Fourier analysis on the $z^\pm(t)$ time series, and only then defined the outward and inward fields, using the daily average of the magnetic field as an estimate for the large-scale field B_R° . This should introduce an error during periods corresponding to sector boundaries where the magnetic field radial component changes sign. However, the percentage of days containing sector boundaries is small (less than 10%) and so we expect the consequences of the error to be small on statistics and correlations.

3. DAILY VARIATIONS OF TURBULENT ENERGIES AND OF SOME PLASMA PARAMETERS

An overview of the primary Helios mission is provided in Figure 1 which shows daily averages of some plasma parameters obtained as described above versus time. The two top panels show the heliocentric distance R , the proton density n and, separately, the bulk velocity V . The rise of the density corresponds to a decrease of the heliocentric distance, from 1 AU at the beginning down to the minimum of 0.3 AU around day 93. On the other hand, as time goes on, we see particles which are emitted from different regions on the Sun: the 27 days recurrence of several high-speed

streams is visible on the V curve [see *Rosenbauer et al.*, 1977; *Burlaga et al.*, 1978].

The third panel in Figure 1 shows the turbulent amplitude $\Delta z = \langle \delta v^2 + \delta b^2 \rangle^{1/2}$, and the proton thermal speed c_s , computed on a daily basis. Note that the recurrent stream structure is clearly visible in the Δz and c_s curves. The turbulent amplitude Δz follows the c_s curve well, enhancing the fluctuations somewhat, particularly the maxima. As may be seen on the bottom panel, in which we plot the relative rms proton density fluctuation $\Delta n/n$, the maxima of turbulent amplitude coincide with maxima of $\Delta n/n$ (but the opposite is not true). Note that we have pointed the largest maxima of Δz by circles on the V , Δz and $\Delta n/n$ curves. This is an indication that both c_s and $\Delta n/n$ govern the level of turbulent energy. When comparing the second and third panels, it appears that V does not play such a decisive role in controlling the turbulent level. We will see below that the case of the Alfvén velocity $c_a = | \langle B \rangle / (4\pi\rho)^{1/2} |$ is similar in this respect.

Note that excepting the proton density n the parameters shown in Figure 1 show very strong variations on the short term (on the scale of several days), related to the stream structure, but much less, if any, related to the solar wind expansion. The relatively small variation of Δz with heliocentric distance, compared to the known variation of the magnetic field power in proportion to the power -3.2 of the heliocentric distance R [*Bavassano et al.*, 1982] is due to the normalization with density n which decreases faster than R^{-2} . This makes the use of the z variable (and more generally of energy per unit mass instead of energy per unit volume) more convenient.

To see how the daily fluctuations of the total turbulent energy compare with those of the ingoing and outgoing components, we have plotted on Figure 2 the rms fluctuations in both components Δz^{out} and Δz^{in} , as well as c_s versus time (we thus have $e^{\text{out}} = \langle \Delta z^{\text{out}} \rangle^2 / 2$ and $e^{\text{in}} = \langle \Delta z^{\text{in}} \rangle^2 / 2$; remember also that total energy is $e = (e^{\text{out}} + e^{\text{in}}) / 2$). One can see that the recurrence of periods with dominance of the outward traveling component, i.e. the so-called Alfvénic periods, is related to the flow structure, being found mainly in high-speed streams (see *Belcher and Davis* [1971]; note however that this is not any more the case outside periods of minimum solar activity [*Marsch et al.*, 1981; *Roberts et al.*, 1987]). On the other hand, it is clear that the energy in the inward component is less correlated with proton thermal speed.

To quantify the visual impressions given by Figures 1 and 2, we have fitted (logarithmically) the turbulent specific energies e , e^{out} and e^{in} with the four plasma parameters c_s , V , c_a and $\Delta n/n$. Table 1 gives the correlation coefficients. Note that V , c_a , c_s are related to one another, but appear not to be related to $\Delta n/n$. It is seen that outward (respectively inward) energy is well correlated with proton thermal speed (respectively $\Delta n/n$). Whenever a substantial correlation with V , c_a or c_s occurs, the highest is that with c_s , as already seen in Figure 1: although the flow structure may be an important parameter, the variable V itself is not the most pertinent factor. Since c_s and $\Delta n/n$ are uncorrelated, we conclude that these two quantities are the relevant plasma parameters with which to correlate the turbulent energies. A best fit of these energies with a combination of power laws of the form $c_s^\alpha \{ \Delta n/n \}^\beta$ gives the following results (C denotes the correlation coefficient):

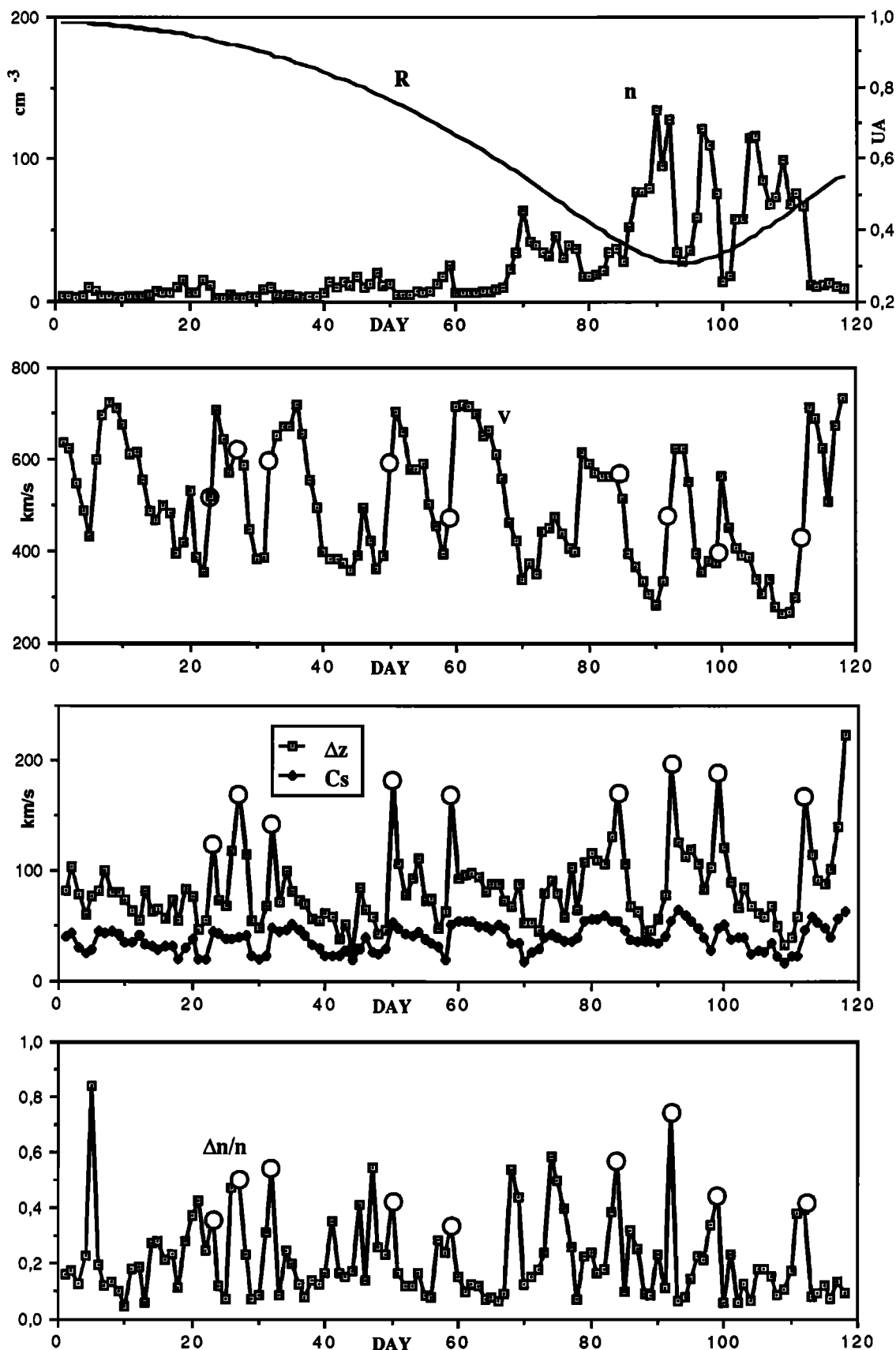


Fig. 1. Synoptic variations of some characteristic quantities (daily averages). Abscissa is time in days, starting from the first day of the Helios mission. From top to bottom: Density n and heliocentric distance R ; bulk velocity V ; proton thermal speed c_s , and rms turbulent speed Δz (calculated from kinetic and magnetic fluctuations); relative rms density fluctuation $\Delta n/n$. Circles highlight days with maximal values of turbulent energy.

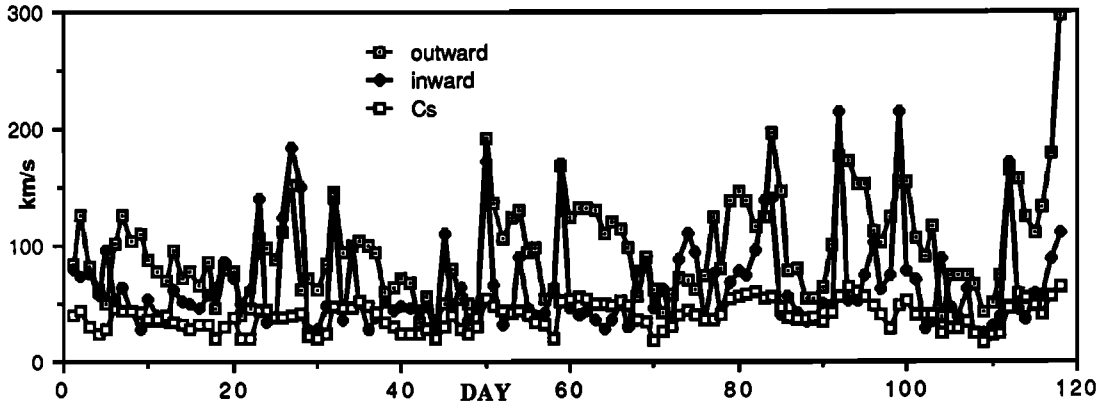


Fig. 2. The rms turbulent amplitudes of the outward and inward components versus day.

Total energy e

$$1.8 \leq \alpha \leq 2 \quad 0.3 \leq \beta \leq 0.4 \quad C=81\% \quad (3a)$$

Outward component e^{out}

$$2 \leq \alpha \leq 2.2 \quad -0.1 \leq \beta \leq 0.1 \quad C=82\% \quad (3b)$$

Inward component e^{in}

$$1 \leq \alpha \leq 1.4 \quad 0.9 \leq \beta \leq 1.1 \quad C=71\% \quad (3c)$$

It is seen by comparing with Table 1 that fitting the energies with both c_s and $\Delta n/n$ gives a better fit, except for e^{out} , which does clearly not depend on $\Delta n/n$.

From equations (3a) and (3c), we may conclude that Alfvénic periods ($e^{out} \gg e^{in}$) appear essentially in regions with high temperature and low $\Delta n/n$, which correspond well to the "trailing edges of high-speed streams" of Belcher and Davis [1971, p.3534].

4. AMPLITUDE AND SHAPE FLUCTUATIONS OF SPECTRA WITHIN STREAM STRUCTURE

Turbulent energies depend obviously on the time scale of integration (here 1 day). Considering periods smaller than one day will change the figures given above. Moreover, the flow structure (via c_s and $\Delta n/n$) should also affect the spectra of the outgoing and ingoing components separately. We shall first describe the intrinsic variations of spectra, and then look for a dependence of these spectra on plasma parameters.

TABLE 1. Cross Correlations Between Turbulent Energies e , e^{out} and e^{in} on the One Hand, With the Main Flow Parameters on the Other Hand

	$\log V$	$\log c_s$	$\log c_a$	$\log \Delta n/n$
$\log c_s$	0.71			
$\log c_a$	0.46	0.74		
$\log \Delta n/n$	-0.23	-0.09	-0.16	
$\log e$	0.54	0.77	0.61	0.19
$\log e^{out}$	0.62	0.82	0.71	-0.08
$\log e^{in}$	0.13	0.33	0.22	0.60

The proton thermal speed is c_s , the Alfvén speed c_a , bulk speed V and rms relative density fluctuations $\Delta n/n$.

4.1. A Qualitative Analysis of the Spectral Variations

Figure 3 gives e^{out} and e^{in} spectra representative of two different periods in the solar wind. Figure 3a (fifth day of Helios mission) corresponds to a local minimum of bulk velocity. The inward and outward traveling components have comparable amplitude, except at the lowest frequencies (octaves 1 to 3), where there is an excess of inward component. The second example in Figure 3b shows the same spectra 3 days later (day 8): at that time, the bulk velocity is twice that of day 5, and is close to a local maximum (see Figure 1). Comparing with Figure 3a, we see that the outward component has risen up at all frequencies, while the inward component has fallen down, so that the outward component is now dominant, mostly in the middle-high frequency range. This systematic "breathing" of the spectra occurs repeatedly as the satellite successively encounters the recurrent streams. Figure 4 shows a series of sample spectra found respectively in peaks of velocity (top panel) and just in front of the peaks (bottom panel), together with the correspondence with the bulk velocity pattern (middle panel).

The sample spectra shown in Figure 4 are extreme examples, chosen for illustrative purpose, but they do not

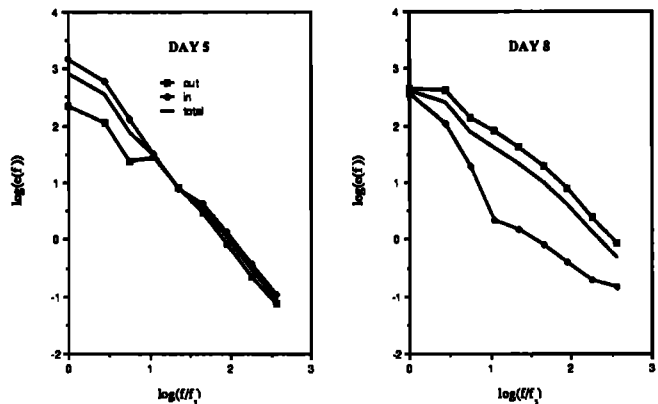


Fig. 3. Two typical energy spectra $e(f)$ for ingoing and outgoing waves, normalized to $1(\text{km/s})^2 \text{d} = 8.64 \times 10^4 (\text{km/s})^2 \text{Hz}^{-1}$: the same normalization will be used in all figures. Frequency is normalized to $f_1 = \text{d}^{-1}$: (left) day 5, a low velocity region, and (right) day 8, in a high-speed stream.

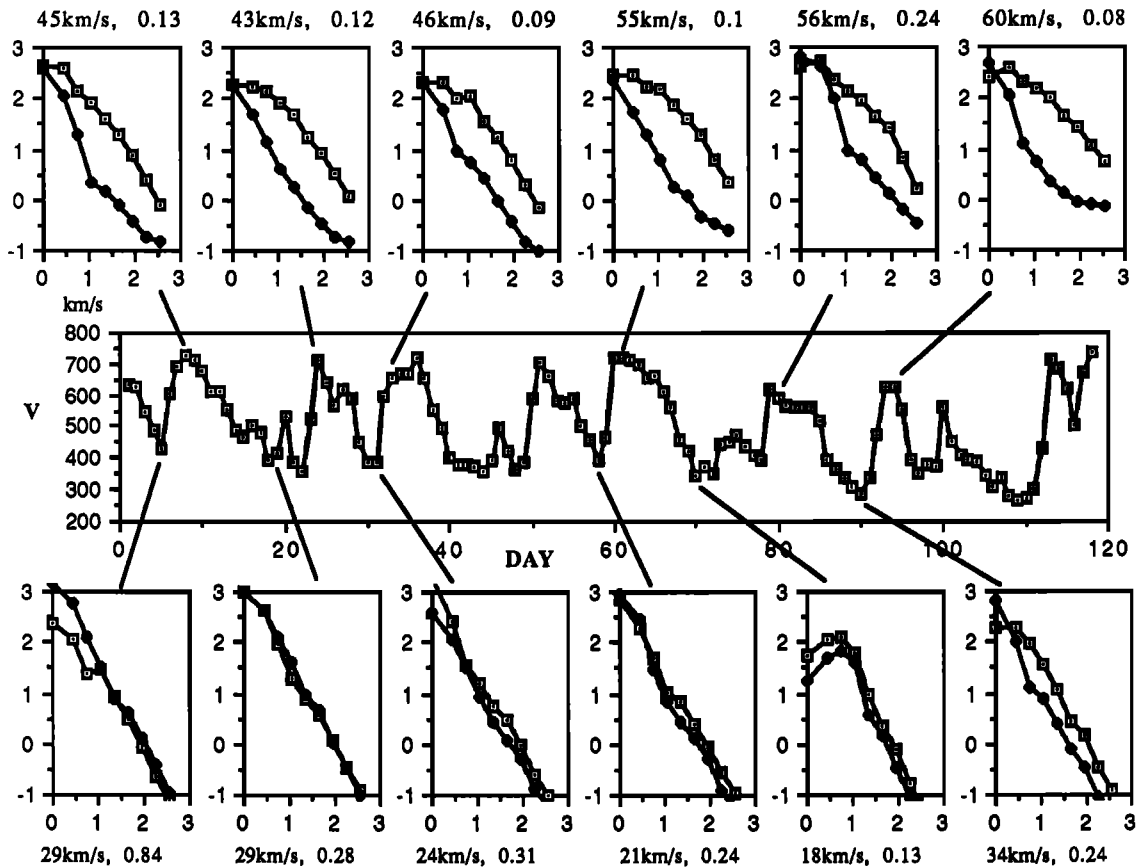


Fig. 4. Some sample spectra in high-speed streams and interaction regions. Abscissa is time in days and ordinate is average bulk velocity. The small panels show energy spectra for the outgoing component $e^{\text{out}}(f)$ (squares) and for the ingoing component $e^{\text{in}}(f)$ (same units as in Figure 3). Numbers above top panels and under bottom panels indicate the proton thermal velocity c_s and the rms relative density fluctuation $\Delta n/n$.

indicate how the spectra evolve between these extrema. It is not practical to plot all daily spectra versus frequency. A first, qualitative impression of the evolution of spectra is given in plate 1, which is essentially a three-dimensional representation of the turbulent energies (each level is represented by a color) as a function of frequency (in ordinate, from channel 1 to 9) and time (in abscissa). The plate shows three spectra (from bottom to top): outgoing component, ingoing component and relative density fluctuations, and superimposed, the three quantities: proton temperature T , rms relative density fluctuations $\Delta n/n$ and heliocentric distance R . To grasp the meaning of the plate, consider a given energy level E_* , represented by a given color, and define a frequency f_*^{out} , such that $e^{\text{out}}(f_*^{\text{out}}) = E_*$ (and a similar definition for f_*^{in}). The plate shows both that the frequency f_*^{out} (for each energy level E_*) follows in time the c_s curve while f_*^{in} follows $\Delta n/n$. This indicates that the shape of the spectra do not vary very much while the overall amplitude follows either c_s or $\Delta n/n$.

The same phenomenon is illustrated in a more quantitative way in Figure 5, which shows the energy densities $e_i^{\text{out}}(t)$ and $e_i^{\text{in}}(t)$ in the nine frequency channels versus time. For the sake of comparison, we also plot in Figure 5 the proton thermal speed c_s and relative density fluctuation level $\Delta n/n$. Large (2 order of magnitude) variations on the scale of the stream structure (1-6 days) are observed. Visual inspection shows two types of patterns superimposed: spike patterns, similar to those found in the $\Delta n/n$ curve, and more regular sawtooth patterns, similar to that of c_s , or also of V (see

Figure 1). Depending on the frequency and the field considered, one pattern is dominant. For instance, for the outgoing component, spikes are frequent at low frequencies, while the sawtooth pattern is shown by the medium-high frequencies.

4.2. Self-Similarity of the Fluctuations

If the turbulent level at a given frequency depends preferentially on c_s or on $\Delta n/n$, depending on the frequency and type of field (inward or outward), then one should be able to separate the time dependence from the frequency dependence in the spectral variations. If true, this property has of course to be reconciled with the large changes in global spectral shapes apparent in Figure 4.

Time dependence. The amplitude of the variations are very large, about a factor 100 (see Figure 5), which should be compared with the factor four exhibited by the bulk energy $V^2/2$ of the wind (see top of Figure 1). However, the high frequencies show remarkably similar variations, in frequency bands 4 to 9. The strongest property which we can look for is that of self-similarity, which is achieved when the spectral shape does not depend on time, i.e. when the spectrum is of the form $e(f,t) \propto H(t)E(f)$.

Frequency dependence. The examples of Figure 4 show that spectra are systematically bent at the beginning of high-speed streams, which seems to preclude the existence of any permanent power law in the spectrum. More details are shown in Figure 5. Note that power laws would appear as

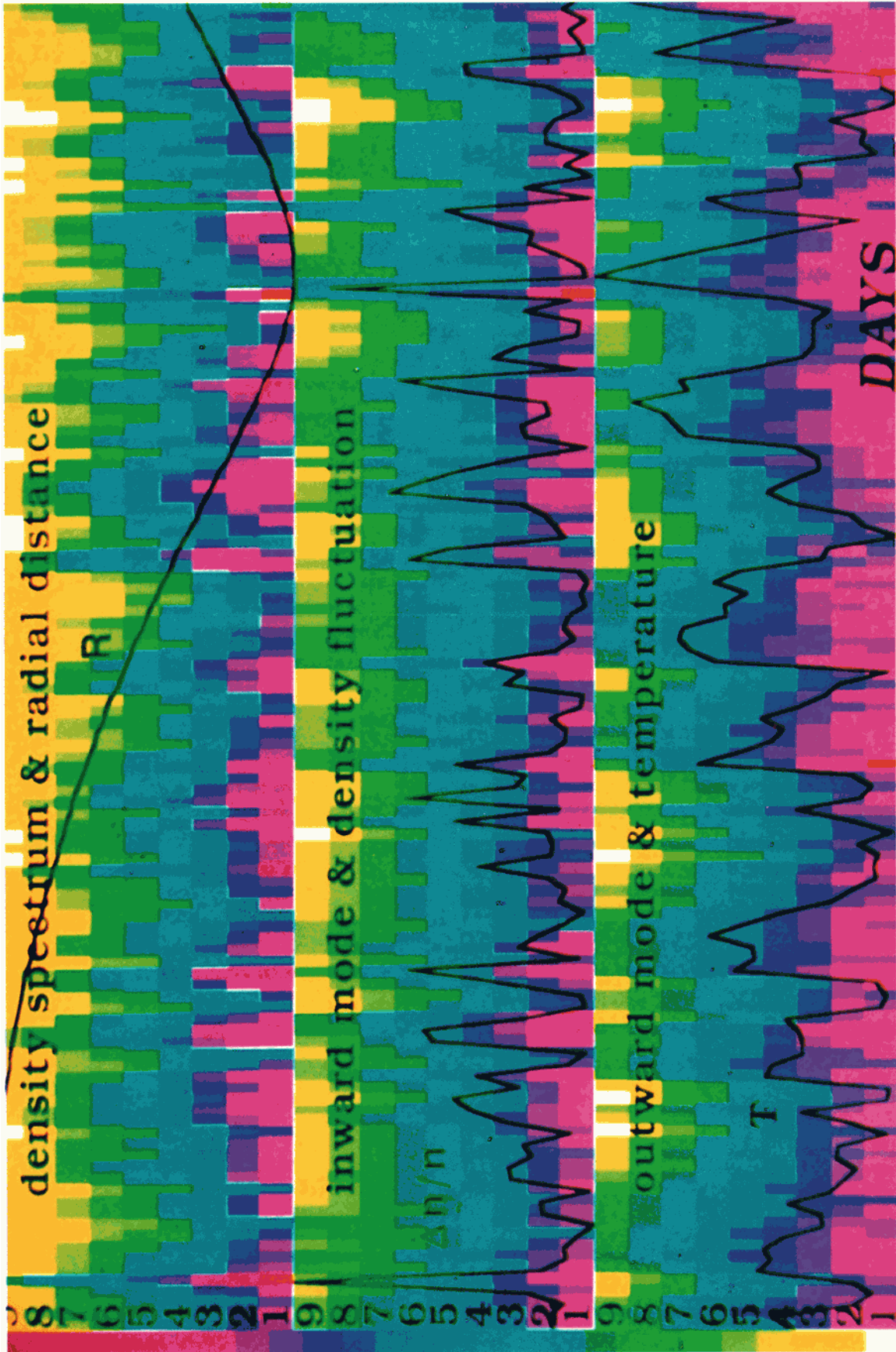


Plate 1. Daily fluctuations of turbulent spectra during the first 118 days of Helios primary mission. From top to bottom, relative density spectrum, spectra of inward and outward components. Abscissa is time in days, ordinate is frequency band (see equation (1)). Colors indicate the energy level in (arbitrary) logarithmic units. Superimposed on each panel are (from top to bottom, in arbitrary units) the heliocentric distance R , the rms relative density fluctuation $\Delta n/n$ and the proton temperature T .

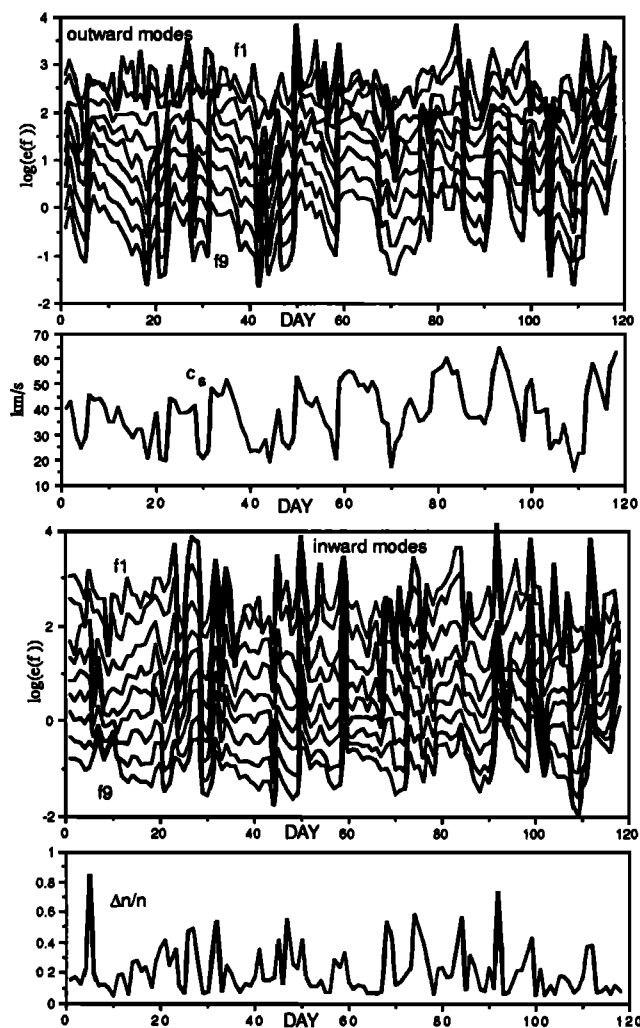


Fig. 5. Daily fluctuations of spectral densities. (Top) Turbulent energy density of the outward component e_i^{out} in the nine frequency bands $i=1$ to 9, and proton thermal speed c_p . (Bottom) The rms relative density fluctuation $\Delta n/n$, and turbulent energy of ingoing modes e_i^{in} in octaves $i=1$ to 9. Abscissa is day, ordinate unit is as in Figure 3.

equally spaced curves for successive octaves. The curves corresponding to the lowest frequencies are sometimes more closely packed and sometimes less than those corresponding to the high frequencies, indicating that there is no unique

slope for the whole spectrum. Visual inspection indicates, however, that the high-frequency range (octaves 4 to 9) might follow a power law dependence with frequency. We will use in the following as synonyms scale invariance and power law dependence.

In order to check quantitatively the self-similarity property, we have made a linear fit of the daily energy densities between successive frequency octaves; namely, we have determined the coefficients A and B which lead to the best fit of the linear relation: $\log(e_i) = A \log(e_{i-1}) + B$ for octaves $i=2$ to 9. If fluctuations are self-similar, then A has to be nearly unity. If A is exactly unity, then $B/\log 2 = \{ \langle \log(e_i) \rangle - A \langle \log(e_{i-1}) \rangle \} / \log(f_i/f_{i-1})$ is a measure of the local (in frequency, but time averaged) slope of the spectrum. Note, however, that small deviations of A from unity makes $B/\log 2$ very different from the actual slope: we will thus not use it for slope measurements.

Table 2 shows the correlation coefficients between successive octaves, as well as the coefficients A and B . The correlation coefficients are rather high in the frequency bands 3 to 9 for the outward and total energies, and in the whole spectrum for the inward component. Except for the lowest two frequency bands, the values of A are generally close to 1. However, A is systematically and significantly lower than unity for the inward component (except for the last band), and greater than unity for the outward component, in frequency bands 4 to 9. A value of A smaller than unity implies that the energy in high frequencies varies less than the energy in the lower frequencies, in other words that the slope of the spectrum steepens when the energy in the inward component is higher. Thus the outward and total energy spectrum are systematically flatter when their amplitude is larger, and the contrary for the inward spectrum (except for band 9): Figure 4, although it is a somewhat biased selection of extreme examples, exhibits some of this average behavior.

We have already seen in Figure 5 that the outward and inward components fluctuate rather independently one from the other, except perhaps for the highest frequencies. Table 3 shows the cross-correlation coefficients, frequency band by frequency band, between both components. On the one hand, the cross-correlation coefficient at the same frequency band i , i.e., between e_i^{in} and e_i^{out} , is always low (lower than 0.3) in the bands $i=3$ to 6. On the other hand, the only large correlations (larger than 80%) are found in band 9 of inward

TABLE 2. Best Logarithmic Fit Between Energy Densities e_i at Successive Frequency Octaves $i=2$ to 9: $\log(e_i) = A \log(e_{i-1}) + B$

	i							
	2	3	4	5	6	7	8	9
e								
Cor	0.85	0.73	0.86	0.91	0.97	0.98	0.99	0.99
A	0.61 ± 0.03	0.69 ± 0.06	0.97 ± 0.05	1.04 ± 0.04	1.06 ± 0.02	1.09 ± 0.02	1.08 ± 0.01	1.04 ± 0.01
B	0.75 ± 0.09	0.28 ± 0.14	-0.33 ± 0.10	-0.44 ± 0.07	-0.44 ± 0.03	-0.50 ± 0.02	-0.51 ± 0.01	-0.44 ± 0.01
e^{out}								
Cor	0.77	0.74	0.86	0.93	0.97	0.99	0.99	0.99
A	0.55 ± 0.04	0.82 ± 0.07	1.01 ± 0.06	1.06 ± 0.04	1.07 ± 0.02	1.07 ± 0.02	1.07 ± 0.01	1.02 ± 0.01
B	0.97 ± 0.12	0.05 ± 0.17	-0.37 ± 0.12	-0.45 ± 0.07	-0.45 ± 0.03	-0.49 ± 0.02	-0.52 ± 0.01	-0.46 ± 0.01
e^{in}								
Cor	0.90	0.83	0.90	0.91	0.95	0.95	0.92	0.95
A	0.69 ± 0.03	0.77 ± 0.05	0.88 ± 0.04	0.86 ± 0.04	0.87 ± 0.03	0.97 ± 0.03	0.98 ± 0.04	1.04 ± 0.03
B	0.44 ± 0.08	-0.13 ± 0.11	-0.31 ± 0.06	-0.28 ± 0.04	-0.31 ± 0.02	-0.40 ± 0.01	-0.43 ± 0.02	-0.31 ± 0.02

Cor is the correlation coefficient between $\log(e_i)$ and $\log(e_{i-1})$. Standard error estimates are given.

TABLE 3. Cross Correlation Between Logarithms of Energy in Outward and Inward Components in the Nine Frequency Bands

i_{in}	i_{out}								
	1	2	3	4	5	6	7	8	9
1	0.56	0.40	0.14	0.03	0.08	0.09	0.11	0.12	0.12
2	0.54	0.48	0.23	0.10	0.11	0.11	0.12	0.12	0.12
3	0.37	0.40	0.31	0.17	0.13	0.11	0.10	0.08	0.06
4	0.33	0.37	0.31	0.20	0.16	0.13	0.12	0.10	0.09
5	0.40	0.45	0.39	0.27	0.29	0.26	0.25	0.24	0.22
6	0.39	0.46	0.44	0.34	0.35	0.35	0.34	0.32	0.31
7	0.37	0.50	0.56	0.48	0.50	0.50	0.50	0.49	0.47
8	0.36	0.56	0.68	0.65	0.69	0.70	0.71	0.71	0.69
9	0.39	0.60	0.74	0.74	0.81	0.82	0.83	0.84	0.84

The variables i_{out} are the frequency octaves for outgoing component, i_{in} are frequency octaves for ingoing component.

component, and bands 5 to 9 of the outward component. More generally, if we consider any fixed band $i>1$ for the outward spectrum e^{out} and look in the table for correlation with the ingoing spectrum e^{in} , we find that the maximum correlation is always found at the band $j=9$. Such a correlation between excitation of opposite modes at widely separated scales is reminiscent of the nonlocal (in wave number space) coupling between opposite modes found in homogeneous MHD by Grappin *et al.* [1982] and Grappin [1986], which was invoked to explain the cascade of velocity-magnetic correlation e^c towards small scale with sign reversal, and hence the growth of correlation in the long term [see also Matthaeus *et al.*, 1983].

4.3 Variation of the Turbulent Spectra With c_s and $\Delta n/n$

Let us now look at how the relation between turbulent energies and the parameters c_s and $\Delta n/n$ actually depends on the frequency band. We have done for each frequency band a logarithmic fit of the form

$$e(f) \propto (c_s)^\alpha (\Delta n/n)^\beta \quad (4)$$

The quality of the fit is indicated on Table 4 and illustrated in Figure 6. Table 4 shows that the correlation is larger than 80% for the outward and total energies in the

high-frequency bands (5 to 9). It is always lower for the inward component, but it remains everywhere larger than 60%, except for band one of the outward component. This means that the variation in c_s and $\Delta n/n$ are responsible for a very substantial part of the turbulent fluctuations in the frequency domain we are considering. Note that if the factor $\Delta n/n$ can be forgotten for e and e^{out} at high frequencies, it plays an important role at low frequencies for e and e^{out} , and is the dominant factor for e^{in} up to frequency band 6.

In Figure 6, we compare the fits and the data for e_5 and e_9 (Figure 6a) and for e^{in}_2 , e^{in}_5 , e^{in}_9 (Figure 6b). Figure 6a (for which we have neglected the $\Delta n/n$ dependence) shows that the fit follows closely the data in the frequency bands 5 to 9 on medium and large time scales: most of the time, the fit is within a factor 2 of the data, which is small compared to the overall variation of the turbulent level. As concerns e^{in} , the fit is clearly not so good, (except for the frequency band 9), the deviations being a substantial fraction of the total amplitude variation.

Figure 7 shows how α and β vary when the frequency varies: both parameters show large and significant variations from the values obtained by fitting the integrated energies. There are two cases where β is approximately constant, however. First, $\beta \approx 1$ in bands 1 to 5 for inward energy, so that $e^{in}(f) \propto \Delta n/n$. Second, toward large frequencies, $\beta \approx -1/3$, thus slightly negative for e^{out} , and compatible with zero for

TABLE 4. Cross-Correlation Coefficients Between the Spectral Densities in the Nine Frequency Bands on the One Hand and Proton Thermal Speed c_s , the rms Relative Density Fluctuations $\Delta n/n$ and Both Quantities Together on the Other Hand

	i								
	1	2	3	4	5	6	7	8	9
					$\log e$				
$\log c_s$	0.36	0.49	0.68	0.78	0.86	0.89	0.90	0.91	0.90
$\log \Delta n/n$	0.48	0.44	0.16	0.01	-0.07	-0.14	-0.15	-0.18	-0.20
Both	0.63	0.69	0.72	0.79	0.86	0.89	0.90	0.91	0.91
					$\log e^{out}$				
$\log c_s$	0.39	0.60	0.73	0.78	0.84	0.87	0.88	0.90	0.89
$\log \Delta n/n$	0.28	0.14	-0.10	-0.18	-0.18	-0.22	-0.21	-0.23	-0.24
Both	0.51	0.63	0.73	0.79	0.85	0.88	0.89	0.91	0.90
					$\log e^{in}$				
$\log c_s$	0.26	0.25	0.19	0.18	0.33	0.41	0.54	0.72	0.81
$\log \Delta n/n$	0.52	0.61	0.60	0.58	0.56	0.46	0.37	0.15	0.02
Both	0.61	0.68	0.65	0.63	0.68	0.64	0.69	0.75	0.81

The variable e is total energy spectrum (kinetic plus magnetic), e^{out} and e^{in} are the outward and inward component energy spectra, respectively.

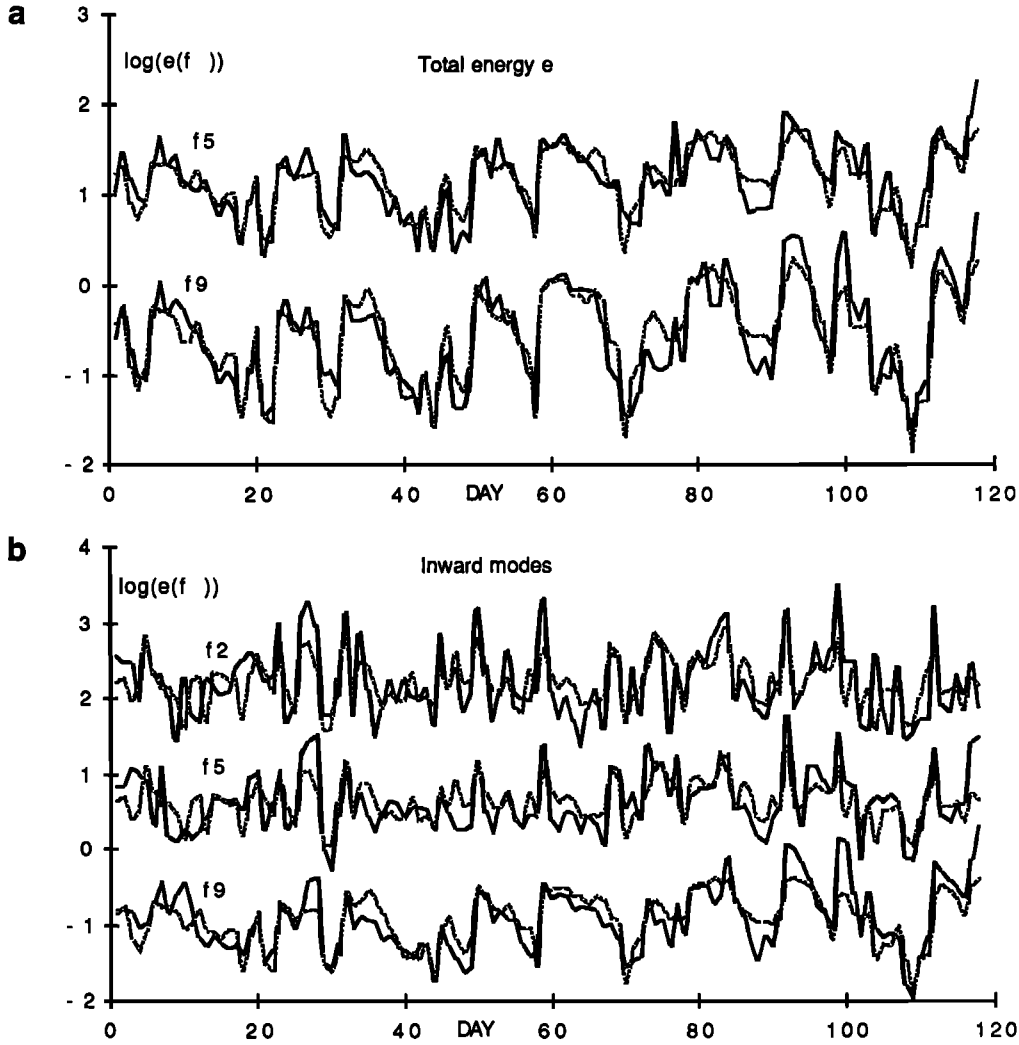


Fig. 6. Comparison of the data with the prediction of a logarithmic fit with c_s and $\Delta n/n$: (a) total energy e in bands 5 and 9 (fit with c_s only), and (b) inward component's energy e^{in} in bands 2, 5 and 9 (fit with both c_s and $\Delta n/n$). Solid line indicates original data, and dashed line is result of the fit.

total energy, indicating that at these frequencies e is insensitive to the variation of $\Delta n/n$.

Except for these two cases, both α and β vary strongly with frequency, and so the shape of the spectra will in general vary continuously with the plasma parameters. Let us try to summarize these variations. When the temperature rises at constant $\Delta n/n$, e and e^{out} essentially rise at all frequencies, but more at high than low frequencies: thus their spectrum becomes flatter. As for e^{in} , it rises less at frequency f_4 than at other frequencies, the result being that the spectrum becomes flatter at higher frequencies and steeper at lower frequencies: thus one should find a break in the inward spectrum at high temperature in this frequency band, as is indeed found (see Figure 4). When the rms density fluctuation rises at constant temperature, the inward component's spectrum becomes steeper (the same is true for e and e^{out} , but only at low frequencies).

In the high-frequency part, in bands 5 to 9, these variations take a simple form: α and β are both approximately linear functions of $\log(\text{frequency})$ for the three energies. Thus if there is a power law spectrum for any particular couple (c_s , $\Delta n/n$), the spectrum will still be power law for other values of both parameters, although with a

slope. We give in Figure 8 the spectral fits for the two days 5 ($c_s=29$ km/s, $\Delta n/n=0.20$) and 8 ($c_s=45$ km/s, $\Delta n/n=0.13$), corresponding to the original data already plotted in Figure 3. We note that in bands 5 to 9 the spectra are reasonably well represented by power laws. Approximating the α and β variations by the straight continuous lines indicated in Figure 6, we obtain

$$e(f) \approx 10^{-2.7} \times c_s^{2.5} (ff_5)^m$$

$$m \approx -3.0 + \log c_s \quad (5a)$$

$$e^{\text{out}}(f) \approx 10^{-3.2} \times c_s^{2.8} [\Delta n/n]^{-0.2} (ff_5)^m$$

$$m \approx -3.0 + \log c_s \quad (5b)$$

$$e^{\text{in}}(f) \approx 10^{0.46} \times c_s^{1.1} [\Delta n/n]^{0.85} (ff_5)^m$$

$$m \approx -3.6 + 1.2 \log c_s - 0.6 \log (\Delta n/n) \quad (5c)$$

These formulas illustrate quantitatively the effect of the variation of c_s and $\Delta n/n$ on the slopes of all spectra. As c_s varies from 16 km/s to 63 km/s, the slope of both e and e^{out} varies from -1.8 to -1.2. As for e^{in} , the slope varies from -2.1 to -0.8 corresponding to the extreme values $c_s=16$ km/s, $\Delta n/n=0.8$, and $c_s=63$ km/s, $\Delta n/n=0.06$.

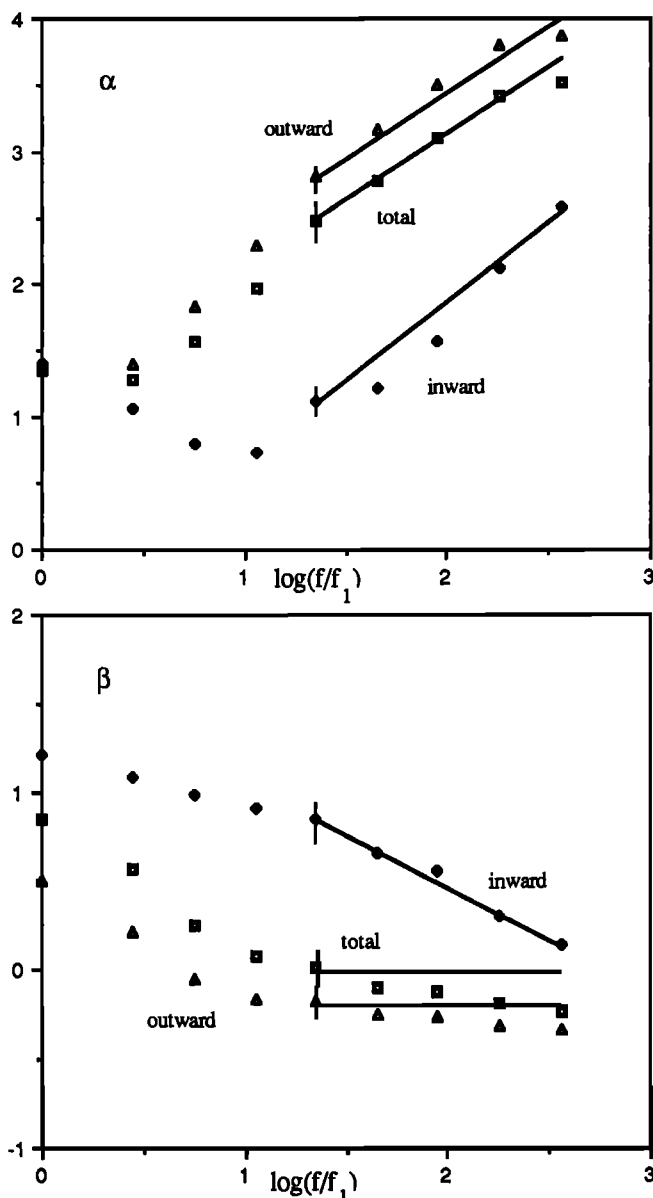


Fig. 7. Variations of power indices α and β for the three energy spectra (e , e^{out} and e^{in}) obtained by fitting logarithmically these quantities with c_s and $\Delta n/n$, versus frequency: $e(f) \propto c_s^\alpha (\Delta n/n)^\beta$.

Since c_s and $\Delta n/n$ vary almost independently from one another, as suggested by their low correlation coefficient (9%, see Table 1), one would expect that the spectra of e^{out} and e^{in} vary in a somewhat erratic way. Now, we have seen in section 4.2 that from bands 4 to 9, e^{out} becomes flatter when its level rises, and the opposite for e^{in} . Thus the variations of c_s and $\Delta n/n$ are in fact related in some subtle way, perhaps in the long term, as may be visually inferred from Figure 1. In particular, to obtain the "breathing" of the e^{out} and e^{in} spectra illustrated by Figure 4, it is clear that $\Delta n/n$ and c_s must vary in opposite sense. Indeed, at the days illustrated in the upper panels of the figure, c_s is systematically larger, and $\Delta n/n$ smaller, than the values at the days illustrated in the bottom panels.

5. DISCUSSION

Our main findings can be summarized as follows. While the specific turbulent energy is strongly varying from day to

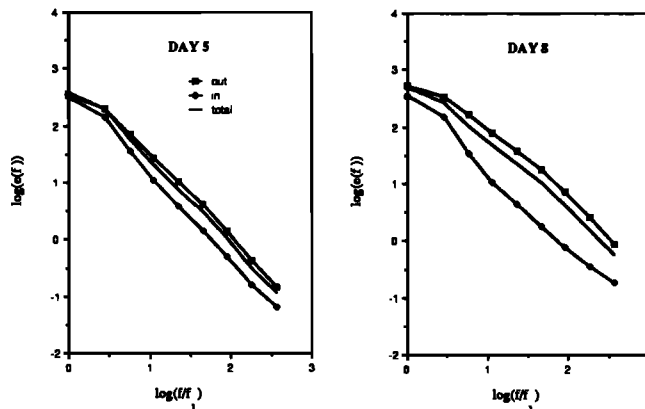


Fig. 8. Predictions of the fit with c_s and $\Delta n/n$ for the spectra e , e^{out} and e^{in} at days 5 and 8 (see Figure 3 for the original data).

day, with variations of more than 2 orders of magnitude, a large part of these variations seems to be accounted for by the variations of only two large-scale parameters. The first one, the proton thermal speed c_s , characterizes the internal state of the solar wind plasma; the second one, $\Delta n/n$, describes the degree of compressibility of the turbulence.

The total specific turbulent energy of the outward component, integrated over the whole frequency band (1.2×10^{-5} , 6×10^{-3}) Hz, depends only on c_s ($e^{\text{out}} \propto c_s^2$), while the inward component depends more strongly on $\Delta n/n$, $e^{\text{in}} \propto c_s \Delta n/n$. As a result, the total specific energy (kinetic plus magnetic) behaves mainly as e^{out} , but has a slight dependence on $\Delta n/n$, $e^{\text{total}} \propto c_s^2 (\Delta n/n)^{1/3}$. (It should be kept in mind that our logarithmic fits of e^{out} , e^{in} and e with c_s and $\Delta n/n$ have no reason to respect the relation $e = (e^{\text{out}} + e^{\text{in}})/2$; they can only be expected to give fits of e which will be lying somewhere between e^{out} and e^{in}).

According to this, Alfvénic periods (where $e^{\text{out}} \gg e^{\text{in}}$) are found in regions where c_s is large, and $\Delta n/n$ is small, which is not contradictory with the observations by *Belcher and Davis* [1971] that they are found in the trailing edges of high-speed streams. On the other hand, it now has been demonstrated by *Marsch et al.* [1981] and *Roberts et al.* [1987] that, outside of solar minimum times, slow wind is frequently as Alfvénic as the fast wind of solar minimum. If our observations are to be still valid outside of solar minimum times, then during these periods, the relative density fluctuations should be small and c_s large. It would be interesting in this respect to reanalyze, for example, the data from *Voyager* and from other periods of Helios 1 and 2.

We have further found that the spectra of outgoing and ingoing modes show very systematic changes of their global spectral shapes when going throughout the stream structure. These changes appear as a kind of "breathing" which repeats itself each time a high-speed stream is encountered: while both spectra are comparable in front of the stream, the outgoing spectrum very rapidly rises with velocity, while the ingoing mode, on the contrary, is depressed. This phenomenon does not result from a direct anticorrelation between both components: cross correlations between both fields at a given frequency are in fact very low, and never negative (see Table 2). It results, on the one hand, from the correlation of the outward (respectively inward) component with c_s (respectively $\Delta n/n$), and on the other hand from the (gross, not detailed) anticorrelation of c_s with $\Delta n/n$,

compressive turbulence occurring essentially in front of high-speed streams, and the proton thermal temperature following (grossly again) the bulk velocity structure.

More precisely, the present observations show that the spectral shapes are not independent of the global level of turbulent energies and that the two parameters c_s and $\Delta n/n$ "control" both the energy level and the spectral shapes. In the high frequency domain where the correlations are the highest, (from 2×10^{-4} to 6×10^{-3} Hz), the spectra have a power law dependence on the frequency, but with spectral indices depending on c_s and $\Delta n/n$ (see equation (5)). In the particular case of total energy, the variation of the spectral index may be represented by a simple law, $m = -3 + \log(c_s)$.

The spectral index m thus varies in this spectral range from -1.2 for a "hot" wind ($c_s \approx 63$ km/s) to -1.8 for a "cool" wind ($c_s \approx 16$ km/s). This variation of m on the scale of a few days is comparable to the variation with distance found by several authors [see *Bavassano et al.*, 1982; *Denskat and Neubauer*, 1982]. If we use a linear fit of $\log c_s$ with heliocentric distance R for the particular period of 120 days considered here, we obtain $\log c_s = 1.68 - 0.16R$, leading to the following variation of m with R : $m = -1.32 - 0.14R$. Thus from 0.3 AU to 1 AU, the average slope m varies from 1.37 to 1.47: this is thus much smaller than the results mentioned above, which were obtained by considering the whole Helios mission. This discrepancy may come in part from the fact that we are looking at the total specific energy, while previous authors consider only the magnetic energy. More probably, it comes from the fact that the period of 4 months considered here is a period of solar minimum with specific properties. Indeed, comparing the above temperature variation with distance with the results by *Marsch et al.* [1982], *Schwenn* [1983], *Freeman* [1988], based on 6 years of Helios data, we find that the radial gradients are much larger on this larger period. For instance, if we use the best fit obtained by *Freeman* [1988] for wind velocity between 300 and 400 km/s, which can be written $\log(c_s) \approx 1.2 - 0.6 \log R$, we obtain for the slope $m = -1.7 - 0.6 \log R$, hence a larger variation range, m varying from -1.4 to -1.7.

At low frequencies, the correlation with $\Delta n/n$ becomes significant, and larger than that with c_s for the inward component, but the part of the total energy variation explained by both c_s and $\Delta n/n$ becomes somewhat smaller. It is worthwhile to note that in bands 1 to 5 (10^{-5} to 4×10^{-4} Hz), $e^{in(f)} \propto \Delta n/n$. This is reminiscent of the so-called "pseudosound" relation predicted for weakly compressible turbulence [*Montgomery et al.*, 1987]. On the other hand, *Passot and Pouquet* [1987] have observed in their numerical simulation of two-dimensional Navier-Stokes decaying turbulence that an "acoustic regime" of turbulence dominated by compressive modes develops as soon as the initial density fluctuation is high enough. The compressible turbulence we observe here could be an MHD version of this "acoustic regime" of turbulence.

The c_s and $\Delta n/n$ variations do not explain all the variation in turbulent energies, especially the large peaks which are signaled by circles in Figure 1. These peaks are strongest in the lowest frequencies (see Figure 5), and occur almost only in the vicinity of sector boundaries, in compression regions, with large velocity variations. The parameter $\Delta n/n$ exhibits also large peaks in these regions (whereas c_s does not), but not of sufficient amplitude to explain all the turbulent

variation through the fit of equation (3). This suggests that other parameters may play a role as for example some measure of the velocity gradient.

6. CONCLUSION

Here are some partial answers to the questions we raised in the introduction:

1. One cannot define two clear-cut regimes of solar wind turbulence, i.e., either Alfvénic or non-Alfvénic; instead there is a continuous variation from day to day. For total (kinetic plus magnetic) energy e in the frequency range (1.2×10^5 , 6×10^{-3} Hz), this variation may be described simply as a rising up and down from steep spectra in the cold wind to flat spectra in the hot wind.

2. Solar wind turbulence is not of a different nature at 0.3 AU and at 1 AU. On the contrary, it shows the same variations with the large-scale properties of the wind at both distances: at high frequencies, the radial variation simply results from the average cooling of the wind between 1 AU and 0.3 AU. Both the slope and cross-helicity variations can be accounted for by variations of temperature.

3. Is what we observe the result of nonlinear, or linear (WKB-like) processes? On the one hand, we are not aware of any nonlinear process in which the proton temperature controls both the level and the slope of the turbulent spectrum. On the other hand, if the spectral variations on the scale of a few days were the result of the expansion, then we would have to explain why the proton temperature and turbulent amplitude follow each other so well. This is in fact an analogous (but even more difficult) problem to that of explaining why the temperature is higher when the velocity of the wind is higher, although one would expect that a maximum velocity would lead to stronger expansion effects, i.e., stronger cooling; this is partially explained by invoking an enhanced dissipation of waves in high-speed streams [*Freeman*, 1988].

A possible scenario is suggested by the remark made by [*Freeman*, 1988, p.90], that "the very low-speed wind escapes the wave heating, probably by originating from regions of the corona where MHD wave emission is prohibited, i.e., non-coronal holes or at the borders of holes." If we accept this idea, the turbulence in the wind originating from coronal holes (i.e., the fast streams) will be essentially Alfvénic, i.e., dominated by the outward component. On the contrary, the turbulence in slow winds originating from closed regions outside coronal holes is not fed by the solar surface, but can only result from local sources, which do not particularly favor the outward component.

Velli et al. [1989] have suggested that in the case of a strongly Alfvénic turbulence in a slowly varying medium the nonlinear flux is different from that used for instance by *Tu et al.* [1984], so that the competition between MHD and WKB effects will produce a k^{-1} spectrum, instead of leading asymptotically to the steeper Kolmogorov or Kraichnan spectra. In more general situations there will be a competition between this nonlinear flux and the more standard one (Kraichnan or Kolmogorov-type) and, as proposed by *Velli et al.* [1990], this last flux will dominate at large heliocentric distance, thus leading to pure Kolmogorov or Kraichnan spectra.

Combining these latter ideas with the former by *Freeman* [1988], we propose that regions originating from coronal

holes will be Alfvénic, have flatter spectra and a larger turbulence level, and the opposite for the other regions. In the Alfvénic regions, the dissipation rates will also be larger, due to higher excitation levels at high frequencies. This will explain the high correlation between turbulent parameters and proton thermal speed, if we assume the existence of a (hypothetical) mechanism ensuring a one-to-one equilibrium relation between turbulent energy flux and temperature. In order to account for the fact that this correlation appears to hold as well at 0.3 than at 1 AU, this mechanism should be at work, not only close to the solar corona, but also all the way during transport by the wind.

Extending this scenario to other periods, such as those covered by the whole of Helios mission or Voyager mission, is not immediate, and probably asks for reanalyzing these data. Let us make two final remarks. We have seen that the period of solar minimum which we have studied corresponds to very low radial gradients of temperature. This seems to indicate large heating rates, and thus more Alfvénic periods, according to our scenario. We are not aware of any work showing such a difference. On the other hand, transient periods, which appear often in periods of solar maximum, show globally steeper spectra [Goldstein *et al.*, 1984], which is in favor of lower heating rates. Now we have already noted that Freeman [1988] finds radial gradients of temperature much larger than ours. This may be attributed to the fact that the period he considers contains a period of solar maximum, during which heating rates are smaller.

Acknowledgments. We thank H. Rosenbauer and F. M. Neubauer for making the merged Helios data available for this study. We acknowledge several interesting discussions with J. Léorat, C. Tu, M. Velli and P. L. Veltri. We warmly thank one of the referees (D. A. Roberts) for many interesting remarks and stimulating criticism, and in particular for pointing out to us that the method of interpolating the data which we used in the first version of this paper was inappropriate.

The Editor thanks A. Barnes, T. E. Holzer, and D. A. Roberts for their assistance in evaluating this paper.

REFERENCES

- Bavassano, B., M. Dobrowolny, F. Mariani, and N. F. Ness, Radial evolution of power spectra of interplanetary Alfvénic turbulence, *J. Geophys. Res.*, **87**, 3617, 1982.
- Belcher, J. W., and L. Davis, Large-amplitude Alfvén waves in the interplanetary medium, *J. Geophys. Res.*, **76**, 3534, 1971.
- Burlaga, L. F., N. F. Ness, F. Mariani, B. Bavassano, U. Villante, H. Rosenbauer, R. Schwenn, and J. Harvey, Magnetic fields and flows between 1 and 0.3 AU during the primary mission of Helios 1, *J. Geophys. Res.*, **83**, 5167, 1978.
- Coleman, P. J., Turbulence, viscosity, and dissipation in the solar wind plasma, *Astrophys. J.*, **153**, 371, 1968.
- Denskat, K. U., and F. M. Neubauer, Statistical properties of low-frequency magnetic field fluctuations in the solar wind from 0.29 to 1.0 AU during solar minimum conditions: Helios 1 and Helios 2, *J. Geophys. Res.*, **87**, 2215, 1982.
- Dobrowolny, M., A. Mangeney, and P.-L. Veltri, Properties of MHD turbulence in the solar wind, *Astron. Astrophys.*, **83**, 26, 1980a.
- Dobrowolny, M., A. Mangeney, and P.-L. Veltri, Fully developed anisotropic turbulence in the solar wind, *Phys. Rev. Lett.*, **45**, 144, 1980b.
- Freeman, J. W., Estimates of solar wind heating inside 0.3 AU, *Geophys. Res. Lett.*, **15**, 88, 1988.
- Goldstein, M. L., L. F. Burlaga, and W. H. Matthaeus, Power spectral signatures of interplanetary corotating and transient flows, *J. Geophys. Res.*, **89**, 3747, 1984.
- Grappin, R., Onset and decay of two-dimensional magnetohydrodynamic turbulence with velocity-magnetic field correlation, *Phys. Fluids*, **29**, 2433, 1986.
- Grappin, R., U. Frisch, J. Léorat, and A. Pouquet, Alfvénic fluctuations as asymptotic states of MHD turbulence, *Astron. Astrophys.*, **105**, 6, 1982.
- Grappin, R., A. Pouquet, and J. Léorat, Dependence of MHD turbulence spectra on the velocity field-magnetic field correlation, *Astron. Astrophys.*, **126**, 51, 1983.
- Grappin, R., A. Mangeney, and E. Marsch, On the origin of solar wind turbulence: Helios data revisited, in *Proceedings of the workshop on Turbulence and Nonlinear Dynamics in MHD Flows*, edited by M. Meneguzzi, A. Pouquet, and P. L. Sulem, p. 81, North-Holland, Amsterdam, 1989.
- Kraichnan, R. H., Inertial range spectrum of hydromagnetic turbulence, *Phys. Fluids*, **8**, 1385, 1965.
- Marsch, E., K. H. Mühlhäuser, H. Rosenbauer, R. Schwenn, and K. U. Denskat, Pronounced proton core temperature anisotropy, ion differential speed, and simultaneous Alfvén wave activity in slow solar wind at 0.3 AU, *J. Geophys. Res.*, **86**, 9199, 1981.
- Marsch, E., K.-H. Mühlhäuser, R. Schwenn, H. Rosenbauer, W. Philipp, and F. M. Neubauer, Solar wind protons: three-dimensional velocity distributions and derived plasma parameters measured between 0.3 and 1 AU, *J. Geophys. Res.*, **87**, 52, 1982.
- Matthaeus, W. H., M. L. Goldstein, D. Montgomery, Turbulent generation of outward traveling interplanetary Alfvénic fluctuations, *Phys. Rev. Lett.*, **51**, 1484, 1983.
- Montgomery, D., M. R. Brown, and W. H. Matthaeus, Density fluctuation spectra in magnetohydrodynamic turbulence, *J. Geophys. Res.*, **92**, 282, 1987.
- Mussman, G., F. M. Neubauer, and E. Lammers, Radial variation of the interplanetary magnetic field between 0.3 AU and 1.0 AU: Observations by the Helios 1 spacecraft, *J. Geophys. Res.*, **42**, 591, 1977.
- Passot T., and A. Pouquet, Numerical simulation of compressible homogeneous flows in the turbulent regime, *J. Fluid Mech.*, **181**, 441, 1987.
- Pouquet, A., M. Meneguzzi, and U. Frisch, Growth of correlations in MHD turbulence, *Phys. Rev.*, **33A**, 4266, 1986.
- Pouquet, A., M. Meneguzzi and P. L. Sulem, Influence of velocity-magnetic field correlations on decaying magnetohydrodynamic turbulence with neutral X points, *Phys. Fluids*, **31**, 2635, 1988.
- Roberts, D. A., M. L. Goldstein, L. W. Klein, and W. H. Matthaeus, Origin and evolution of fluctuations in the solar wind: Helios observations and Helios-Voyager comparisons, *J. Geophys. Res.*, **92**, 12023, 1987.
- Roberts, D. A., and M. L. Goldstein, Simulation of interplanetary dynamical processes, in *Proceedings of the Third International Conference on Supercomputing*, edited by L. P. Kartashev and S. I. Kartashev, p. 370, International Supercomputing Institute, Boston, 1988.
- Rosenbauer, H., R. Schwenn, E. Marsch, B. Meyer, H. Miggenrieder, M. D. Montgomery, K.-H. Mühlhäuser, W. Philipp, W. Voges, and S. M. Zink, A survey of initial results on the Helios plasma experiment, *J. Geophys. Res.*, **42**, 561, 1977.
- Schwenn, R., The "average" solar wind in the inner heliosphere: Structures and slow variations, *Solar Wind 5, Nasa Conf. Publ.*, **CP-2280**, 489, 1983.
- Tu, C., The damping of interplanetary Alfvénic fluctuations and the heating of the solar wind, *J. Geophys. Res.*, **93**, 7, 1988.
- Tu, C., Z. Y. Pu, F. S. Wei, The power spectrum of interplanetary Alfvénic fluctuations: Derivation of the governing equation and its solution, *J. Geophys. Res.*, **89**, 9695, 1984.
- Velli, M., R. Grappin, A. Mangeney, Turbulent cascade of unidirectional Alfvén waves in the interplanetary medium, *Phys. Rev. Lett.*, **63**, 1807, 1989.
- Velli, M., R. Grappin, A. Mangeney, The effect of the large-scale gradients on the evolution of Alfvénic turbulence in the solar wind, in *Plasma Phenomena in the Solar Atmosphere*, edited by M. A. Dubois, Editions de Physique, Orsay, France, in press, 1990.
- R. Grappin and A. Mangeney, Observatoire de Paris-Meudon, UA173 DAEC, F-92190 Meudon, France.
- E. Marsch, Max-Planck-Institut Für Aeronomie D-3411 Katlenburg-Lindau, Federal Republic of Germany.

(Received February 23, 1989;
revised October 17, 1989;
accepted October 27, 1989.)